IOPscience iopscience.iop.org

Home Search Collections Journals About Contact us My IOPscience

X-ray absorption and diffraction study of II–VI dilute oxide semiconductor alloy epilayers

This article has been downloaded from IOPscience. Please scroll down to see the full text article.

2007 J. Phys.: Condens. Matter 19 446201

(http://iopscience.iop.org/0953-8984/19/44/446201)

View the table of contents for this issue, or go to the journal homepage for more

Download details:
IP Address: 129.252.86.83
The article was downloaded on 29/05/2010 at 06:30

Please note that terms and conditions apply.

IOP Publishing — Journal of Physics: Condensed Matter

J. Phys.: Condens. Matter **19** (2007) 446201 (12pp) doi:10.1088/0953-8984/19/44/446201

X-ray absorption and diffraction study of II–VI dilute oxide semiconductor alloy epilayers

F Boscherini[1,7], M Malvestuto[1,8], G Ciatto[2,9], F D'Acapito[3], G Bisognin[4], D De Salvador[4], M Berti[4], M Felici[5,10], A Polimeni[5] and Y Nabetani[6]

[1] Physics Department and CNISM, University of Bologna, viale C. Berti Pichat 6/2, 40127 Bologna, Italy
[2] European Synchrotron Radiation Facility, BP 220, 38043 Grenoble Cedex, France
[3] OGG-INFM-CNR, c/o European Synchrotron Radiation Facility, BP 220, 38043 Grenoble Cedex, France
[4] MATIS INFM-CNR and Physics Department, University of Padova, via Marzolo 8, 35131 Padova, Italy
[5] Physics Department and CNISM, University of Rome 'La Sapienza', Piazzale Aldo Moro 2, 00185 Rome, Italy
[6] Interdisciplinary School of Medicine and Engineering, University of Yamanashi, Takeda 4-3-11, Kofu 400-8511, Japan

E-mail: federico.boscherini@unibo.it

Received 1 July 2007, in final form 4 September 2007
Published 16 October 2007
Online at stacks.iop.org/JPhysCM/19/446201

Abstract

Dilute oxide semiconductor alloys obtained by adding oxygen to a II–VI binary compound are of potential applicative interest for blue-light emitters in which the oxygen content could be used to tune the band gap. Moreover, their properties can be usefully compared to the more thoroughly studied dilute nitrides in order to gain insight into the common mechanisms which give rise to their highly non-linear physical properties. Recently, it has been possible to deposit ZnSeO and ZnSeOS epilayers on GaAs(001), which exhibit a red-shift of the band gap and giant optical bowing.

In order to provide a structural basis for an understanding of their physical properties, we have performed a study of a set of ZnSeO and ZnSeOS epilayers on GaAs by high resolution x-ray diffraction and x-ray absorption fine structure. We have found that the strain goes from compressive to tensile with increasing O and S concentration and that, while all epilayers are never found to be pseudomorphic, the ternary ones exhibit a low relaxed fraction if compared to the ZnSe/GaAs sample. O K-edge x-ray absorption near edge spectra and

[7] Author to whom any correspondence should be addressed.
[8] Present address: ELETTRA, SS 14 km 163.5, Basovizza (Trieste), Italy.
[9] Present address: Synchrotron SOLEIL, L'Orme des Merisiers, Saint Aubin, BP 48, F-91192 Gif sur Yvette CEDEX, France.
[10] Present address: Ecole Polytechnique Fédérale de Lausanne (EPFL), Physics of Nanostructures Laboratory, CH-1015 Lausanne, Switzerland.

0953-8984/07/446201+12$30.00 © 2007 IOP Publishing Ltd Printed in the UK

corresponding simulations within the full multiple-scattering regime show that O is substitutionally incorporated in the host lattice. Zn and Se K-edge extended x-ray absorption fine structure detect the formation of Zn–O and Zn–S bonds; the analysis of these spectra within multiple-scattering theory has allowed us to measure the local structural parameters. The value of Zn–Se bond length is found to be in agreement with estimates based on models of local distortions in strained and relaxed epilayers; an increase of the mean-square relative displacement is detected at high O and S concentration and is related to both intrinsic and extrinsic factors.

1. Introduction

The inclusion within a semiconductor lattice of foreign atoms is a well known method to alter the crystal's physical properties (e.g. the lattice parameter and the band gap). A physical understanding of the structural changes induced by foreign atom inclusion and their connection with the optoelectronic properties are a prerequisite for a full control of the alloying process, which can lead to the engineering of materials properties. Very clear examples of the connection between structure and electronic properties for semiconductors have been reported for concentrated nitrides [1], ZnMgSSe [2] and nitrogen dilute InGaAsN alloys [3, 4].

Semiconductor alloys composed of atoms having similar covalent radius and electronegativity (e.g. InGaAs) usually exhibit physical properties that vary linearly with composition between the limiting values of the binary compounds. Instead, the addition to binary alloys of small quantities of isoelectronic impurities characterized by very different electronegativity and size with respect to the host lattice elements leads to a breakdown of the above picture, the most dramatic illustration of which is often a large band gap bowing.

Recently, ZnSeO alloys having oxygen concentration in excess of 1% have been successfully grown on GaAs(001), in spite of the limited solubility of O in II–VI compounds [5]; these 'dilute oxide' alloys exhibit a red-shift of the band gap and a giant optical bowing. The study of this technologically relevant material, along with others of the same group, is of fundamental interest since it exhibits both similarities and differences with respect to more studied dilute nitrides such as GaAsN, which can be exploited in order to gain a deeper insight into the general mechanisms and effects of the incorporation of isoelectronic impurities into a semiconductor lattice. Besides their potential for the production of blue-light emitters, the study of dilute oxide alloys is thus also motivated by the fact that they represent an important test-bed for the applicability to other compound families of the models developed for explaining the properties of dilute nitrides.

Compared to dilute nitrides the higher difference in electronegativity of the atoms involved in the II–O–VI alloys implies the formation of more polar bonds, which will presumably lead to greater local distortions in the local atomic environment around the impurity. The role of electronegativity differences has been recently highlighted in hydrogenation studies [6, 7] in which it was found that hydrogen passivates O-related defects in ZnTeO but has no discernible effect on ZnSeO.

In an effort to control independently band gap and lattice parameter, one of the present authors has grown ZnSeOS quaternary alloys [8]. Indeed, the effect of small concentrations of S and O on the band gap of ZnSe is expected to be similar, while, compared to wurtzite ZnO, ZnS has a zinc-blende structure and a lattice parameter which is relatively close to that of ZnSe.

Samples with concentrations of O and S up to 2.9% and 10.2%, respectively, were successfully grown in the zinc-blende structure.

Despite the successful growth and interesting optical properties of these materials, an accurate structural characterization is lacking at the moment; it is the purpose of this paper to provide such a structural description using two complementary x-ray methods: high resolution x-ray diffraction (HRXRD) and x-ray absorption fine structure (XAFS). Open issues to be addressed include the strain relaxation of the epilayers, the effective incorporation of the dilute elements in the zinc-blende lattice and their site location (particularly in view of the wurtzite structure of ZnO), and the dependence of the local structure on composition.

HRXRD is a well established method which can accurately determine the long range order of epitaxial layers [9]. By using HRXRD, some of the authors have already investigated the relation between the lattice parameter of (InGa)(NAs) epilayers and their N concentration [10], as well as the lattice parameter variation due to hydrogen irradiation of InGaAsN epilayers; indeed, it has been found that the information collected with HRXRD can be correlated with the possible structure of hydrogen–nitrogen complexes [11, 12]. In the present paper, using HRXRD we have determined the lattice parameters and the strain relaxation for each of the samples.

XAFS is a relatively more recent technique which has now gained recognition as a powerful and reliable tool in the field of semiconductor science. Some of the authors have used XAFS to determine the degree of ordering in InGaAsN alloys [4], the local strain in GaAsN [13] and the effect of hydrogenation on the local structure of GaAsN and InGaAsN [14], and have proposed a structure for the nitrogen–hydrogen complex in hydrogenated GaAsN [15]. In this paper, using XAFS measurements we have determined the site location of O, one of the dilute elements, verified the formation of Zn–O and Zn–S bonds, measured interatomic distances in the first few shells and probed the degree of static disorder.

2. Sample growth and x-ray measurements

ZnSeO and ZnSeOS epilayers were grown by molecular beam epitaxy (MBE) on GaAs(001) substrates, using elemental Zn and Se, ZnS and RF-plasma excited oxygen as sources of Zn, Se, S and O, respectively. RF power was fixed at 50 W for all samples, except for the ZnSe reference. The thickness of ZnSeO epilayers was between 0.73 and 0.85 μm, and that of ZnSeOS was between 2.4 and 3 μm. 100 nm thick buffer layers, for which oxygen was not supplied, were grown on the substrates to avoid surface oxidation of the GaAs. The growth temperature was between 280 and 350 °C for ZnSeO, and 350 °C for ZnSeOS. In order to investigate the structural property dependence on O concentration, we have controlled O concentration by O_2 flow rate, while temperatures of other sources were kept the same. The O_2 flow rate was changed from 0 (ZnSe) to 0.04 ccm for ZnSeO samples, and from 0.02 to 0.08 ccm for ZnSeOS samples.

HRXRD measurements were performed with a Philips X'Pert PRO™ MRD diffractometer equipped with a Bartels Ge(220) four-crystal monochromator and a parabolic mirror; Cu Kα_1 radiation (λ = 1.540 56 Å) was employed. By using a channel-cut Ge (220) analyzer before the detector the angular acceptance was reduced to 12 arcsec (triple axis configuration). Symmetrical and asymmetrical reflections, (004) and (224) respectively, were coupled to obtain the relaxed lattice parameter of the film. In fact, from the analysis of the (004) reciprocal space map (RSM) we quantified the tilt and the lattice parameter along the growth direction ($a_\perp$), and this information was used to extract from the (224) RSM the film lattice parameter in the growth plane ($a_\parallel$). Finally, the relaxed lattice parameter a_{rel} of the epilayer, i.e. the lattice parameter of the free standing film, was obtained by combining $a_\perp$ with $a_\parallel$ using elasticity theory. In the

following, the degree of strain relaxation was quantified by R, defined as

$$R = \frac{a_{\parallel} - a_{sub}}{a_{rel} - a_{sub}} \times 100, \quad (1)$$

where a_{sub} is the lattice parameter of the substrate. $R = 0$ when the film is pseudomorphic to the substrate (i.e. no strain relaxation), while $R = 100$ when the epitaxial constraint is completely removed (complete relaxation).

XAFS measurements were performed at the O, Zn and Se K edges. Measurements at the Zn and Se edges were performed at the GILDA-BM08 beamline [16] of the European Synchrotron Radiation Facility (Grenoble, France), using a dynamically sagittally focusing monochromator [17]. Fluorescence detection was not applicable in this case because of the intense fluorescence lines of the substrate. Instead, the conversion electron yield mode [18] was used: a metal plate anode biased at 100 V was placed $\sim$1 cm from the samples, the experimental chamber was filled with He gas at atmospheric pressure and the drain current from the samples was recorded as a function of energy; this method has sufficient surface sensitivity to greatly reduce the substrate contribution [19]. To further reduce spectral distortions due to the crystallinity of the samples, a rotating sample holder was used. In all cases, measurements were performed in normal incidence, with the electric vector of the impinging x-ray beam in the sample growth plane. Zinc-blende ZnSe and ZnS and wurtzite ZnO polycrystalline powders were measured as reference compounds in the transmission mode.

The local structure of O was probed by O K-edge x-ray absorption near edge structure (XANES), performed at the ALOISA undulator beamline [20] of the ELETTRA laboratory (Trieste, Italy); the intensity of the O Kα fluorescence signal was recorded as a function of energy using a windowless single element HP-Ge detector placed at 90° to the impinging x-ray beam in the horizontal plane. For selected samples, polarization-dependent measurements were performed by varying the angle between the sample normal and the x-ray beam by a rotation of the sample around a vertical manipulator axis. Since O is dilute in these samples, no spectral distortions due to self-absorption effects are expected [21]. At the energy of the O K edge, penetration of the exciting x-ray beam in the sample is considerably less than in the hard x-ray range, so a brief etch in HF prior to measurements was found to be necessary in order to minimize the distortions due to the presence of a surface oxide layer.

3. Results and discussion

In figure 1 we report HRXRD rocking curves around the (004) reflection for all samples; the position of the (004) peak is directly related to the perpendicular lattice parameter $a_{\perp}$, and a comparative analysis of its lineshape is very useful in order to get a structural overview of the set of samples. Apart from the substrate peak, which is taken as the origin of the angular scale, structures due to the epilayer can be clearly identified in all samples. The ZnSe/GaAs sample (0) exhibits a weak peak at negative angles; this signal is representative of the ZnSe layer, which has a greater lattice parameter than that of GaAs. Interference (Pendellösung) fringes are clearly absent in the diffraction pattern: this is the fingerprint of strain relaxation due to the formation of extended defects at the interface between the film and the substrate (the arrow positioned near $-0.205°$ is the position expected for a pseudomorphic ZnSe film). This fact is clear upon inspection of figure 2(a) and, more importantly, figure 2(b), which report, respectively, the (004) and the (224) RSMs of this ZnSe sample. From the (224) RSM it is evident that the substrate and film nodes do not have the same abscissa, that is, they have different $a_{\parallel}$ lattice parameters. Moreover, the great width of the epilayer node clearly visible in the (004) RSM along the $[hh0]$ direction, an RSM feature due to mosaic spread [9], testifies to the presence of extended defects which destroy Pendellösung fringes.

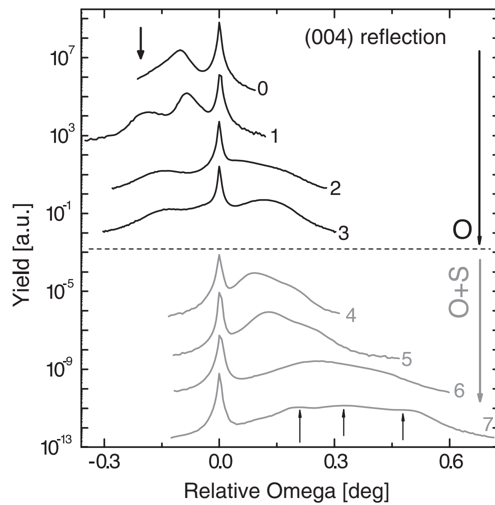

Figure 1. HRXRD (004) rocking curves (RCs) for all the samples. Black lines refer to ZnSe:O doped samples (sample 0 does not contain O), while gray lines represent ZnSe samples doped with both S and O. The three arrows positioned on sample 7 highlight peaks due to strain inhomogeneities of the sample (see the text).

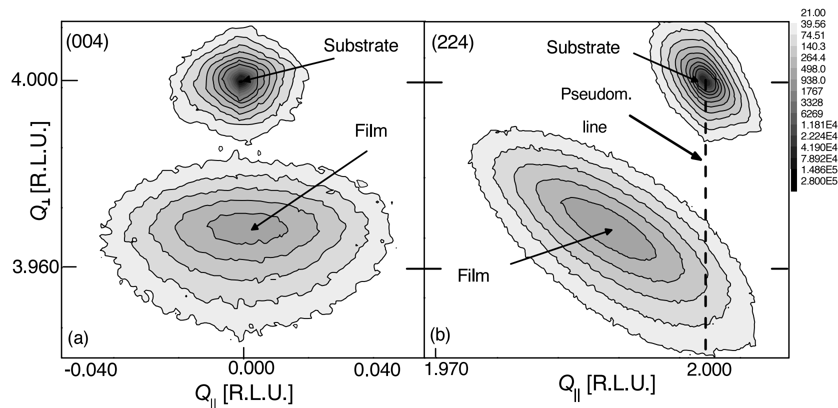

Figure 2. (004) (a) and (224) (b) reciprocal space maps of the ZnSe/GaAs sample (0). Note the distance between the center of the ZnSe node and the pseudomorphicity line (vertical dashed line), which testifies to the strain relaxation of the epilayer.

On addition of oxygen to the ZnSe layer, the (004) peak shifts towards positive angles, indicating strain compensation (the low intensity broad peak centered around $-0.2°$ or less in all RCs is due to the compressive ZnSe buffer layer grown on GaAs in order to prevent GaAs oxidation): this strain compensation is moderate in sample 1, while it is more pronounced in sample 2, in which a broad shoulder at positive angles is clearly visible next to the substrate Bragg peak.

Also in the O-containing samples Pendellösung fringes are absent, demonstrating that the layers are not pseudomorphic to the substrate, even if the addition of O and the consequent lowering of compressive strain towards zero, strongly lowers the value of R measured combining (004) and (224) RSMs, as described before (see table 1).

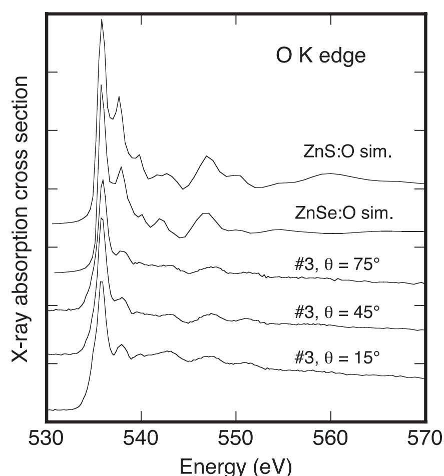

Figure 3. O K-edge polarization-dependent XANES for sample 3 and simulations for an O impurity embedded in ZnSe and ZnS.

Table 1. Sample characteristics and degree of relaxation R determined by HRXRD.

Sample number	Sample code	O concentration (%)	S concentration (%)	R (%)
0	TO050	0	0	94
1	ZSO068	0.9	0	5
2	ZSO130	1.87	0	17
3	ZSO148	2.25	0	7
4	ISO004	0.91	6.75	86
5	ISO006	1.18	7.76	100
6	ISO008	2.86	10.16	—
7	ISO009	5.08	11.08	58–100

Assuming the validity of Vegard's law for the lattice parameter and using [5] $a_{\mathrm{ZnO}} = 4.37$ Å in the cubic structure, from the value of a_{rel} obtained from the (004)–(224) RSMs and using elasticity theory, we estimated the O concentration, which is reported in table 1.

In the lower part of figure 1 the rocking curves of samples doped with both S and O (samples 4, 5, 6 and 7) are reported. All these samples exhibit tensile strain, as expected in view of the rather high concentration of these elements. Also in this case it is important to note the absence of Pendellösung fringes in the spectra, together with a very pronounced broadening and asymmetry of the epilayer peak. While the absence of interference fringes, as previously pointed out, is due to the presence of extended defects that break the pseudomorphicity of the layer, the asymmetry and the broadening of the epilayer peak are indicative of a non-homogeneity of strain (i.e. of the dopants) with depth. The broadening is rather severe for sample 7, in which three peaks can be distinguished from the broad tensile signal (indicated by the arrows): this fact, also verified by RSMs, testifies to the presence of three distinct regions with different associated strain values. The addition of S seems to raise the R values to those of the ZnSe film.

O K-edge XANES spectra were found to be rather similar for all samples. In figure 3 we report polarization-dependent spectra for sample 3 (as a function of the angle between the sample normal and the polarization direction of the incoming photon beam, θ), together with polarization averaged simulations performed in the full multiple-scattering regime for a

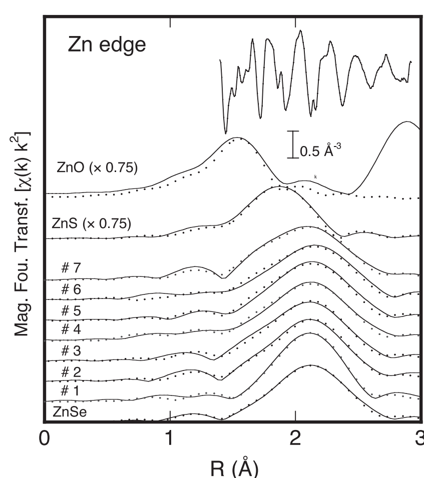

Figure 4. Continuous line, FT of Zn K-edge EXAFS data for all samples; dotted line, fits obtained as described in the text. The inset reports raw EXAFS data for sample 3, in the range 2–12 $Å^{-1}$.

substitutional O atom in a zinc-blende ZnSe or ZnS lattice. Spectra were simulated using the FEFF 8.2 code [22]. The simulations were performed in the full multiple-scattering (FMS) approach using an impurity model where a O atom substitutes either Se or S at the center of a large atomic cluster; clusters consist of 417 atoms for the case of ZnSe:O (i.e. 21 coordination shells around the central O) and of 441 atoms (i.e. 22 shells around O) for the case of ZnS:O. The distances of the nearest and next-nearest neighbors of the central O atom were relaxed by minimizing a valence force field potential [23]. A self-consistency radius (4.2 Å for ZnSe:O, 4.0 Å for ZnS:O) was chosen in order to include all the first and second coordination shell atoms, while the FMS radius was fixed to 13 Å (to include all atoms in the clusters). The polarization dependence of XANES spectra can determine the site symmetry of the absorbing atom, as shown for example in the important case of hexagonal and cubic GaN [24]; in the former case spectra exhibit considerable polarization dependence, while in the latter they are isotropic. The experimental XANES spectra for the three orientations are all quite similar, demonstrating that O has a cubic environment in these samples. Moreover, the good agreement between the experimental spectra and the simulations for a substitutional site convincingly show that this is in fact the site occupied by O.

In figure 4 we report as continuous lines the Fourier transform of the Zn K-edge extended XAFS (EXAFS) data, performed in the range $k = 2$–10 $Å^{-1}$ for the samples and the relevant reference compounds; only the region of the first neighbors is shown, in order to highlight the changes of the lineshape with concentration. The inset shows the raw EXAFS data, to illustrate their quality. The gradual appearance with increasing O (and, to a lesser degree, S) concentration of a low-R tail is evident. This is due to the formation of Zn–O and Zn–S bonds, confirmed by the fitting described below.

In figure 5 we report as continuous lines the Fourier transform of the Se K-edge EXAFS data, performed in the range $k = 2$–10 $Å^{-1}$ for the samples and ZnSe. The inset again shows the raw EXAFS data. We note the similarity of all the spectra, with the evident gradual weakening of the second and third shell contributions (between 3 and 5 Å) with increasing impurity atom concentration.

The EXAFS data were analyzed in the framework of multiple scattering theory using *ab initio* scattering phase shifts and non-linear fitting. As in the case of XANES analyses, FEFF

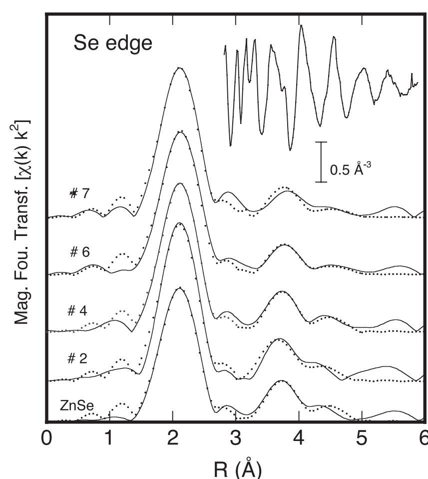

Figure 5. Continuous line, FT of Se K-edge EXAFS data for selected samples; dotted line, fits obtained as described in the text. The inset reports raw EXAFS data for sample 3, in the range 2–12 $Å^{-1}$.

8.2 was used to simulate EXAFS signals at Zn and Se edges. For the Zn edge, simulations were made for ZnO (wurtzite), ZnS, ZnSe and a virtual alloy based on ZnSe and obtained by substituting two of the four Se first shell atoms with an O and a S atom. For the Se edge simulations were made for ZnSe and for the same virtual alloy described above. The ATHENA and ARTEMIS codes [25] were used for quantitative analysis. The first shell was analyzed with a combined fitting of the Zn and Se edge data at the same time, with the following free parameters: two separate energy origin shifts, a single value for the Se–Zn bond length $R_{\mathrm{Zn-Se}}$ and the mean-square relative displacement (MSRD) $\sigma^2_{\mathrm{Zn-Se}}$, an interatomic distance and a MSRD for each of the Zn–O and Zn–S bonds (at the Zn edge); the many-body amplitude reduction factor was fixed to the value found in the preliminary analysis of ZnSe at both edges. Fitting was performed in the ranges $k = 2$–10 $Å^{-1}$, $R = 1.5$–2.7 Å with multiple fitting weights. The low scattering amplitude of O and S posed some limitations to the information which could be gleaned from the data; in particular, it was found to be impossible to fit the value of the Zn–O or Zn–S coordination number so that these values were fixed to the concentration divided by four, the values of the MSRD for Zn–O and Zn–S were fixed to the values found for the bulk compounds and the values for the bond length were found to be affected by a large error (within which, however, they were compatible with the values for the reference compounds). The fittings of the Zn and Se first shells are reported as dots in figures 4 and 5.

The Se edge data were separately analyzed in the region corresponding to the second and third coordination shells ($R = 3$–5 Å). Due to the weakness of the O and S scattering, fits performed with and without S and O in the second shell region were of similar quality and the local structural parameters of Se–Se correlations were found to be identical within the errors. For simplicity we have thus fitted the second shell only with Se. The multiple-scattering signal originating from the Se–Zn–Se three-body atomic arrangement involving the central atom, a Zn first shell and a Se second shell atom was included and its MSRD was fixed to the value for the second shell. Free parameters were the interatomic distances of the second and third shells, their MSRD, and an energy origin shift; the many-body amplitude reduction factor was fixed to the value found in the preliminary analysis of ZnSe while the variation of the multiple-scattering path was calculated based on the value of the first shell bond length and on the

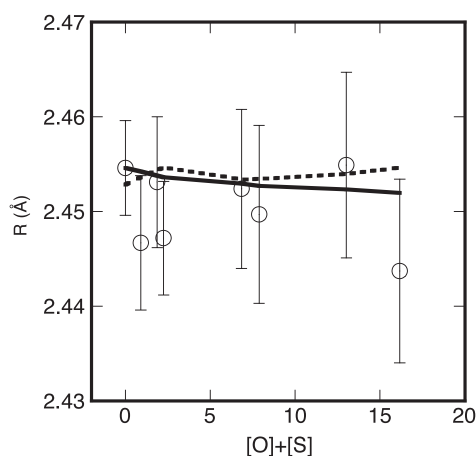

Figure 6. Open dots, values of the Zn–Se bond length as a function of the sum of S and O concentration; the continuous and dashed lines report the theoretical estimates for the pseudomorphically strained and relaxed cases, respectively.

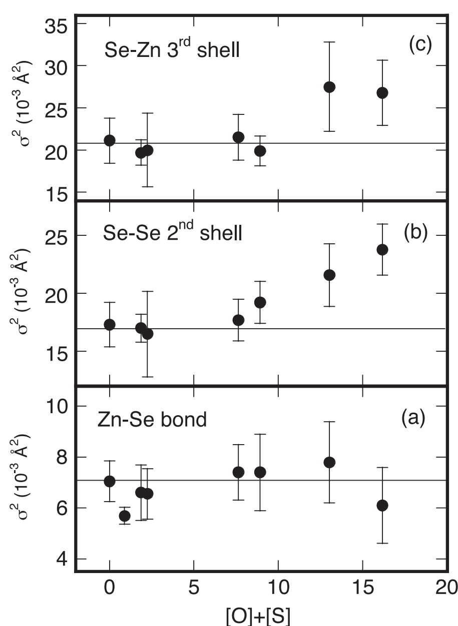

Figure 7. Values of the MSRD for the first three coordination shells around Se as a function of the sum of S and O concentration; the horizontal lines report the values obtained for bulk ZnSe.

variation of the second shell distance. Fitting was performed in the ranges $k = 2.5$–10 Å^{-1}, $R = 3.5$–5.0 Å with multiple fitting weights. The fitting of the second and third shell region for selected samples is shown as dots in figure 5.

We now discuss the values of the most important local structural parameters obtained from the EXAFS analysis. We have made the choice of plotting distances and MSRDs as a function of the sum of the O and S concentration, since this highlights the main trends apparent in the data. Values for interatomic distances for the Zn–Se bond are reported in figure 6 while the values for the MSRDs in the first three coordination shells around Se are reported in figure 7.

The Zn–Se bond length is found to be rather independent of O and S concentration. The effect of strain in thin epilayers on values of bond lengths has been previously studied in detail [26, 27]. Briefly, it has been found that there are two contributions to the variation of bond lengths, which combine linearly to a good approximation: one due to alloying and one due to the strain induced by epitaxial growth; note that these two contributions can have opposite signs. In figure 6, along with the experimental points, we report the estimated values of the bond lengths for pseudomorphically strained and relaxed epilayers. These estimates were performed using a model based on the valence force field theory [23] described in [28] for the relaxed and in [27] for the strained cases. The lattice parameters and C_{11} and C_{12} elastic constants of ZnSe and ZnS were taken from the literature [29]. For ZnO, which is present only in the wurtzite structure, we have calculated *ab initio* the physical constants for the zinc-blende phase using the linearized augmented plane wave (LAPW) method implemented in the WIEN2K code [30]. The muffin tin radii chosen were $R_{MT} = 2.0$ Å for Zn and 1.5 Å for O. The plane wave cutoff parameter $R_{MT} \times k_{max}$ was chosen to be 7. The exchange and correlation effects were treated in the generalized gradient approximation [31]. The Zn 4s and 3d and the O 2p and 2s states were all considered as valence states. The Brillouin zone was sampled with 64 points and the energy convergence criterion was set at 0.0001 Ryd. The elastic parameters were retrieved by using the program ELAST [32] of the WIEN2K package that consists in analyzing the total energy as a function (i) of the cell volume and (ii) of a volume-conservative tetragonal strain. Following this procedure we found a lattice parameter $a_0 = 4.598$ Å, in good agreement with previous theoretical estimates [33], a bulk modulus of $B = 142$ GPa and elastic constants $C_{11} = 171$ GPa and $C_{12} = 127$ GPa. With these data the Zn–Se bond lengths for the ternary compounds $ZnSe_{1-x}S_x$ and $ZnSe_{1-y}O_y$ were calculated and the values for the quaternary compounds were found forming a linear combination of the results using the [O] and [S] concentration as weighting factors. We found that the effect of strain in the examined concentration range is rather small, amounting to at most 0.002 Å. The experimental values are compatible with the estimates of both the relaxed and strained cases, attesting to the validity of our experimental and theoretical procedures; use of the experimental values to study the effect of strain at the local level is hindered by the relatively large value of the error bars.

The values for the MSRDs are reported in figure 7. The first shell values are fairly constant and close to those obtained in the analysis for bulk polycrystalline ZnSe (7×10^{-3} Å^2). The values for the second and third shells are also close to that of ZnSe, except for samples 6 and 7, which exhibit a significant increase. In principle, there may be two origins for this increase in MSRD, the first intrinsic to the material and the second extrinsic (that is, depending on the particular sample structure and morphology). The intrinsic contribution is due to the static disorder induced by the incorporation of O atoms in the host lattice [13]. This can be qualitatively understood as due to the effect on the host lattice of the incorporation of strongly electronegative O atoms; S has no effect since its electronegativity is similar to that of Se. The extrinsic contribution is due to the presence of a range of concentrations for the minor elements in the samples, each local concentration corresponding to a slightly different local environment. It is impossible to decouple these two effects from the XAFS measurements alone; the fact that a significant increase of the MSRD is found for samples 6 and 7 is compatible both with the intrinsic effect (in view of the high O concentration) and with the extrinsic effect (in view of the rather strong inhomogeneities suggested by the HRXRD).

In conclusion, we have presented a structural study of a set of ZnSeO and ZnSeOS dilute oxide epilayers deposited on GaAs(001), using HRXRD and XAFS. The HRXRD results show that strain goes from compressive to tensile with increasing O and S concentration and that, while all epilayers are never found to be pseudomorphic, a low relaxed fraction is exhibited by the ternary samples. O K-edge XANES and corresponding simulations show that O is

substitutionally incorporated in the host lattice. Zn and Se K-edge EXAFS detects the formation of Zn–O and Zn–S bonds and measures the local structural parameters. The Zn–Se bond length is found to be in agreement with estimates based on models of local distortions in strained and relaxed epilayers; an increase of the MSRD is detected at high O and S concentration and is related to both intrinsic and extrinsic factors.

Acknowledgments

Measurements at ESRF were performed within the public user program. Measurements at ELETTRA were supported by Istituto Nazionale per la Fisica della Materia and by ELETTRA. We thank M Capizzi for stimulating discussions.

References

[1] Bellaiche L and Zunger A 1998 *Phys. Rev.* B **57** 4425
[2] Saitta A M, de Gironcoli S and Baroni S 1998 *Phys. Rev. Lett.* **80** 4939
[3] Kim K and Zunger A 2001 *Phys. Rev. Lett.* **86** 2609
[4] Ciatto G *et al* 2003 *Phys. Rev.* B **68** 161201
[5] Nabetani Y, Mukawa T, Ito Y, Kato T and Matsumoto T 2003 *Appl. Phys. Lett.* **83** 1148
[6] Polimeni A, Capizzi M, Nabetani Y, Ito Y, Okuno T, Kato K, Matsumoto T and Hirai T 2004 *Appl. Phys. Lett.* **84** 3304
[7] Felici M, Polimeni A, Capizzi M, Nabetani Y, Okuno T, Aoki K, Kato T, Matsumoto T and Hirai T 2006 *Appl. Phys. Lett.* **88** 101910
[8] Nabetani Y, Ito Y, Mukawa T, Okuno T, Kato T, Matsumoto T and Hirai T 2004 *Phys. Status Solidi* b **241** 595
[9] Holy V, Pietsch U and Baumbach T 1988 *High Resolution X-Ray Scattering from Thin Films and Multilayers* (*Springer Tracts in Modern Physics* vol 149) (Berlin: Springer)
[10] Bisognin G, De Salvador D, Mattevi C, Berti M, Drigo A V, Ciatto G, Grenouillet L, Duvaut P, Gilet P and Mariette H 2004 *J. Appl. Phys.* **95** 48
[11] Polimeni A *et al* 2003 *Phys. Rev.* B **68** 085204
[12] Bisognin G *et al* 2006 *Appl. Phys. Lett.* **89** 61904
[13] Ciatto G, D'Acapito F, Sanna S, Fiorentini V, Polimeni A, Capizzi M, Mobilio S and Boscherini F 2005 *Phys. Rev.* B **71** 115210
[14] Ciatto G, Renevier H, Proietti M G, Polimeni A, Capizzi M, Mobilio S and Boscherini F 2005 *Phys. Rev.* B **72** 085322
[15] Ciatto G, Boscherini F, Amore Bonapasta A, Filippone F, Polimeni A and Capizzi M 2005 *Phys. Rev.* B **71** 201301
[16] D'Acapito F *et al* 1998 *ESRF Newslett.* **30** 42
See also http://www.esrf.fr/exp_facilities/BM8/handbook/control.html
[17] Pascarelli S, Boscherini F, d'Acapito F, Hrdy J, Meneghini C and Mobilio S 1996 *J. Synchroton Radiat.* **3** 147
[18] Kordesh M E and Hoffman R W 1984 *Phys. Rev.* B **29** 491
Guo T and den Boer M L 1985 *Phys. Rev.* B **31** 6233
Tourillon G, Dartyge E, Fontaine A, Le Monnier M and Bartol F 1987 *Phys. Lett.* A **121** 251
Bouldin C E, Forman R A and Bell M I 1987 *Phys. Rev.* B **35** 1429
[19] Erbil A, Cargil G S III, Frahm R and Boheme R F 1988 *Phys. Rev.* B **37** 2450
Schroeder S L M, Moggridge G D, Ormerod R M, Rayment T and Lambert R M 1995 *Surf. Sci.* **324** L371
[20] Floreano L, Naletto G, Cvetko D, Gotter R, Malvezzi M, Marassi L, Morgante A, Santaniello A, Verdini A and Tomasini R 1999 *Rev. Sci. Instrum.* **70** 3855
[21] Carboni R, Giovannini S, Antonioli G and Boscherini F 2005 *Phys. Scr.* T **115** 986
[22] Ankudinov A L, Ravel B, Rehr J J and Conradson S D 1998 *Phys. Rev.* B **58** 7565
[23] Keating P N 1966 *Phys. Rev.* **145** 637
[24] Katsikini M, Paloura E C and Moustakas T D 1996 *Appl. Phys. Lett.* **69** 4206
Katsikini M, Paloura E C and Moustakas T D 1998 *J. Appl. Phys.* **83** 1437
Ciatto G, Boscherini F, d'Acapito F, De Salvador D, Batchelor D, Carboni R, Grenoulliet L, Mariette H and Mobilio S 2005 *Phys. Scr.* T **115** 356
[25] Ravel B and Newville M 2005 *J. Synchroton Radiat.* **12** 537

[26] Romanato F, De Salvador D, Berti M, Drigo A V, Natali M, Tormen M, Rossetto G, Pascarelli S, Boscherini F, Lamberti C and Mobilio S 1988 *Phys Rev.* B **57** 14619
[27] D'Acapito F 2004 *J. Appl. Phys.* **96** 369
[28] Balzarotti A, Motta N, Kisiel A, Zimnal-Starnawska M, Czyzyk M and Podgorny M 1985 *Phys. Rev.* B **31** 7526
[29] Martin R M 1970 *Phys. Rev.* B **1** 4005
[30] Schwarz K, Blaha P and Madsen G K H 2002 *Comput. Phys. Commun.* **147** 71
[31] Perdew J P, Burke K and Ernzerhof M 1996 *Phys. Rev. Lett.* **77** 3865
[32] Package ELAST by Charpin T 2001 http://www.wien2k.at/reg_user/textbooks/elast-UG.ps
[33] Jaffe J E and Hess A C 1993 *Phys. Rev.* B **48** 7903